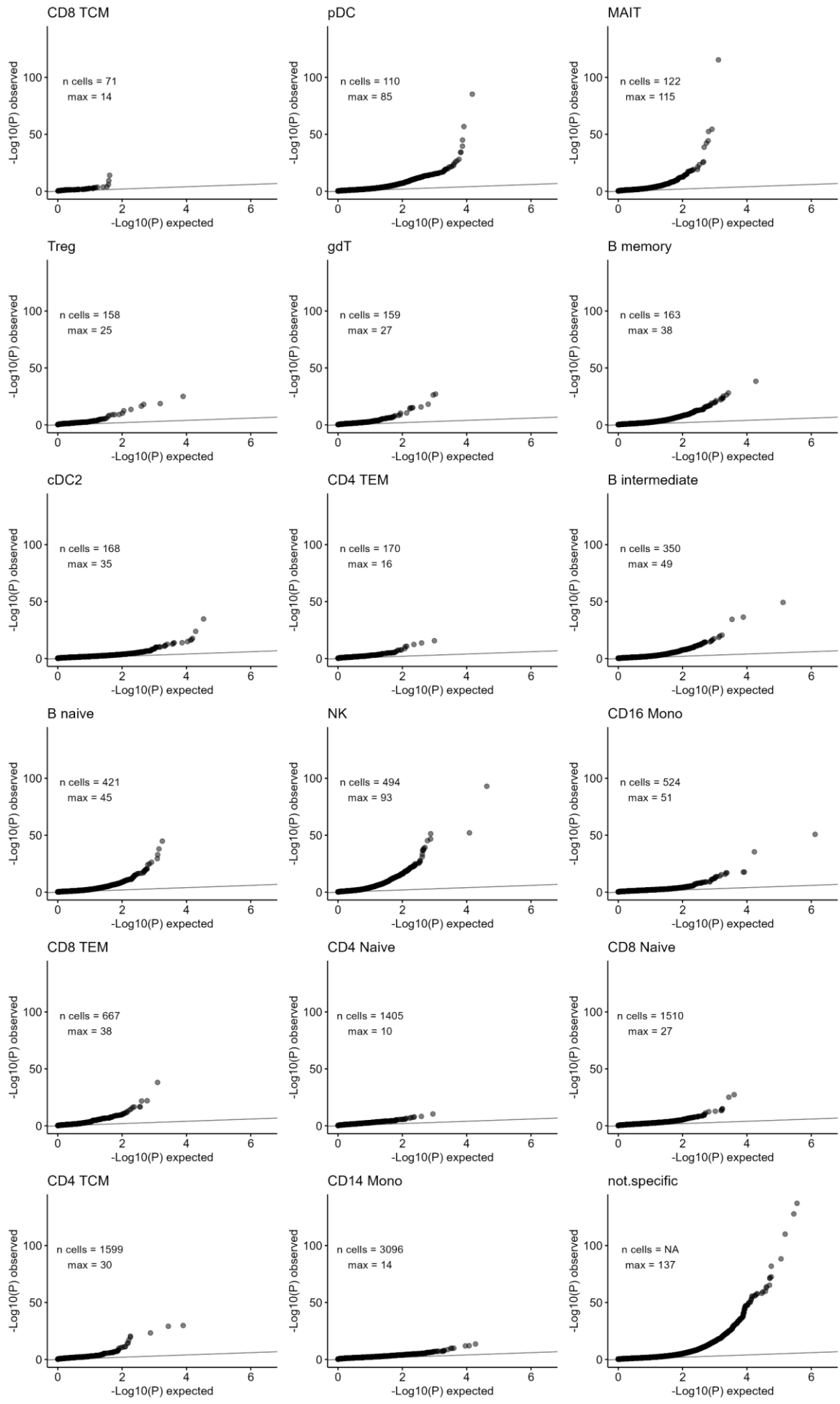
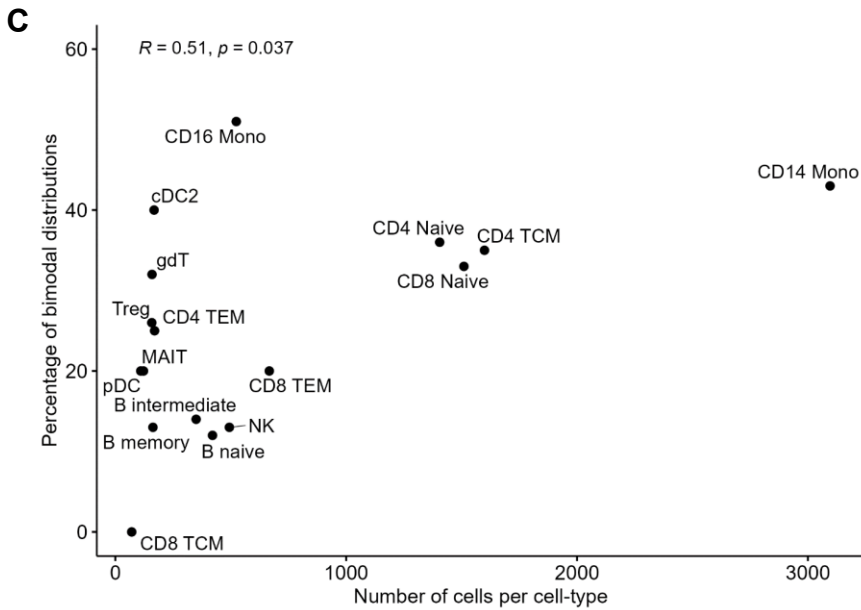
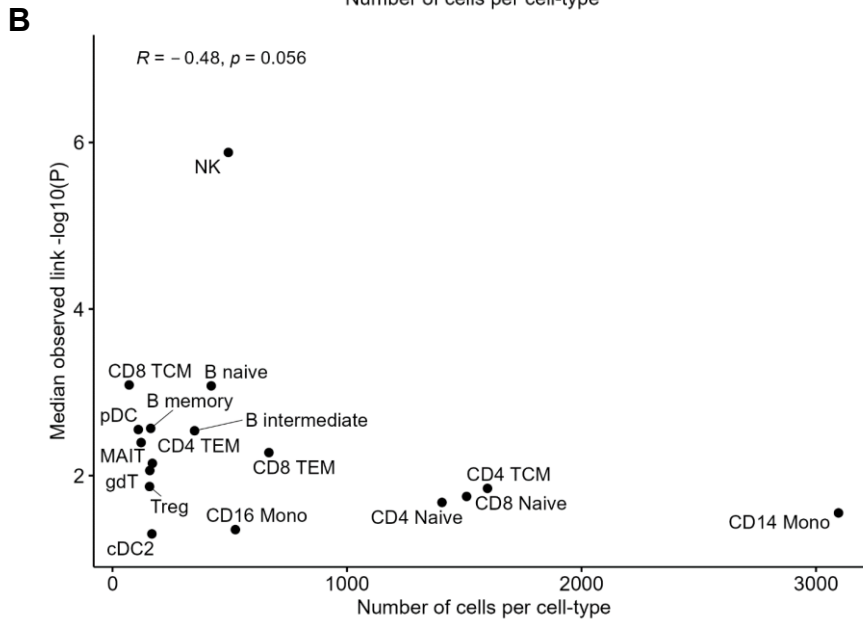
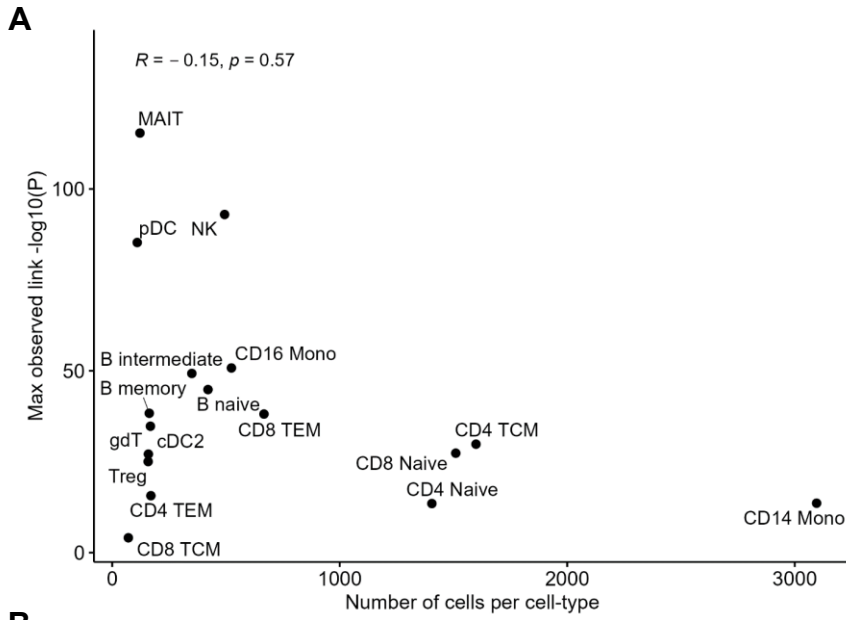


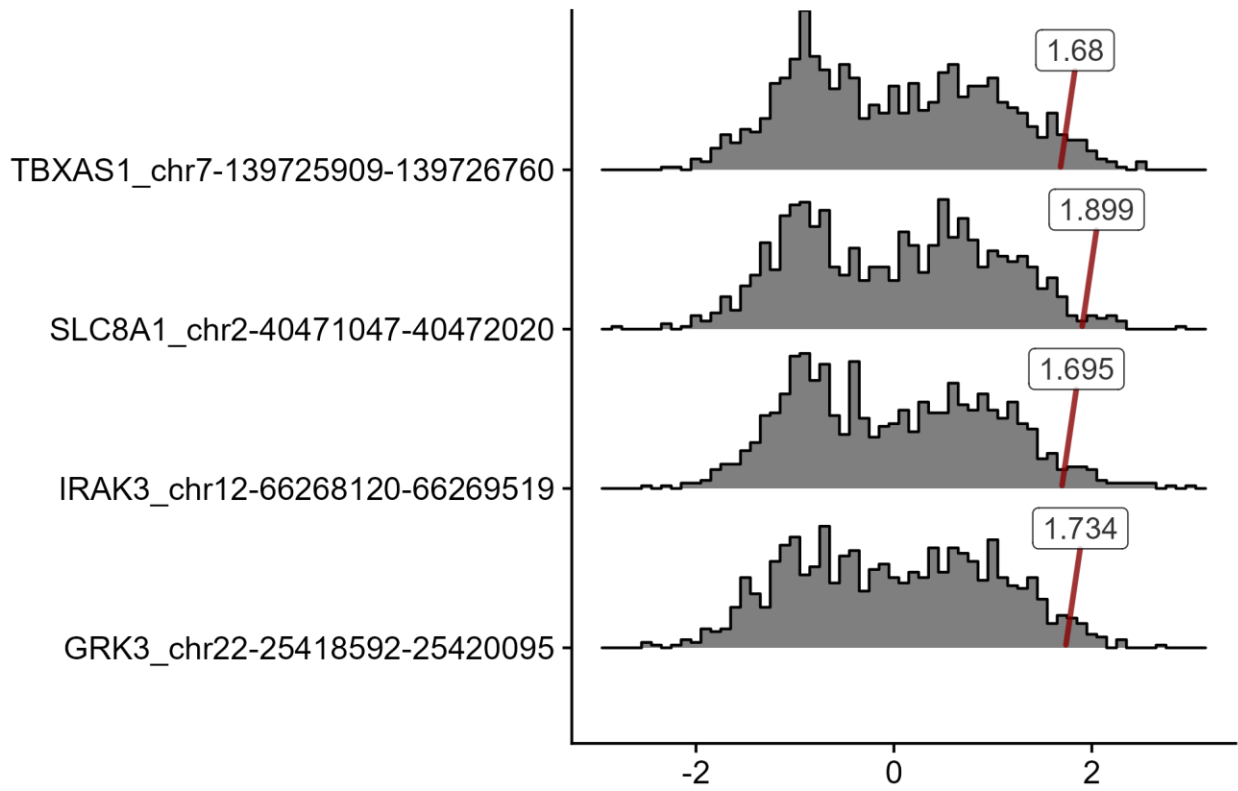
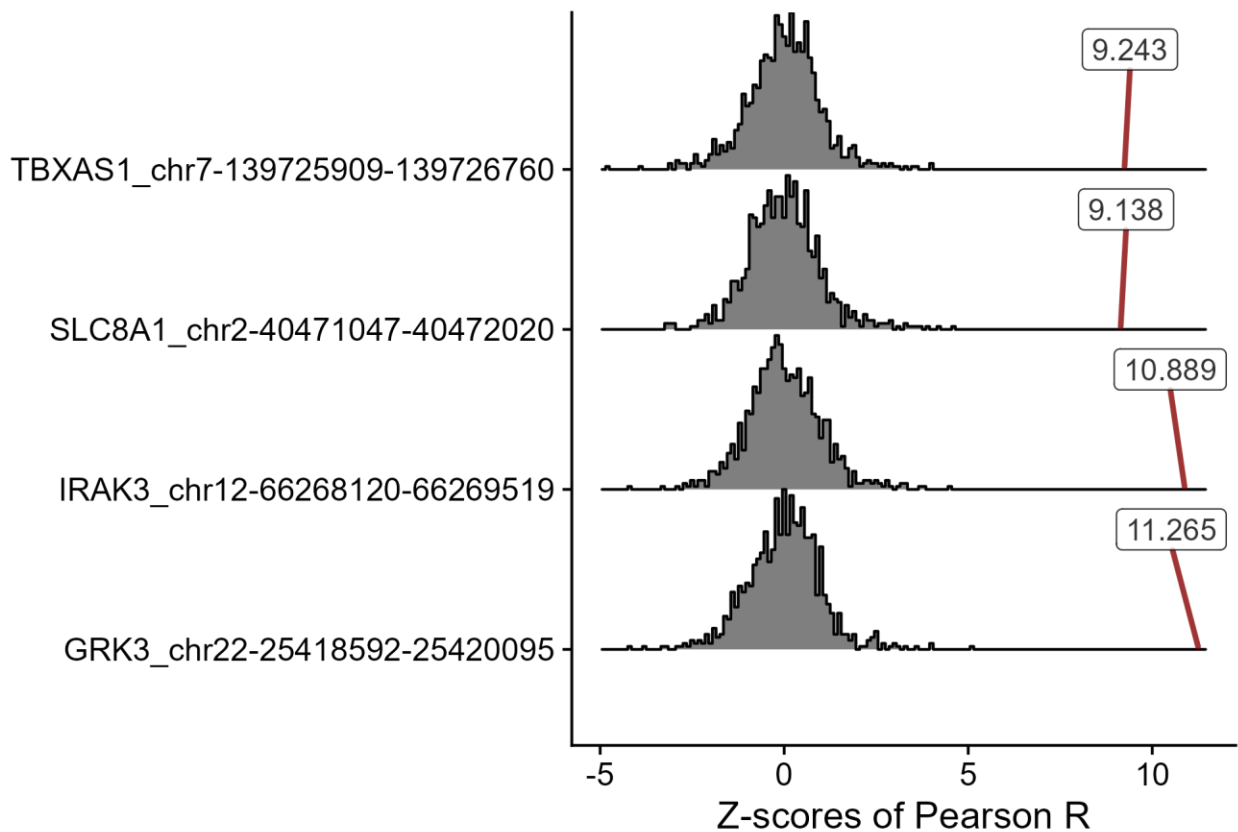
Supplementary Figure 1. Clustering of 11,331 PBMC using (A) ATACseq and (B) RNAseq data. The data is embedded using uniform manifold approximation and projection (UMAP). The Euclidean distance of mean expression by cell-type represented as dendrogram shows mononuclear phagocytes as a distinct cell archetype (CD14, CD16 and cDC2).



Supplementary Figure 2. Distributions of ATACseq peaks-gene link statistics calculated using the Z-scores method as implemented in Signac. The peak-gene links with $|\text{Pearson } R > 0.01|$ were attributed to specific cell-type (cell-types with $n > 50$ cells) using the peak's specificity of accessibility (**Methods**). Mono; Monocytes, cDC; classical Dendritic cells, NK; Natural killer cells, pDC; progenitor Dendritic cells, TEM; T effector memory cells, TCM; T central memory cells, gdT; Gamma delta ($\gamma\delta$) T cells, MAIT; mucosal-associated invariant T cells, Treg; regulatory T cells, Max; maximal $-\log_{10}(\text{P-value})$ calculated for a given cell-type.

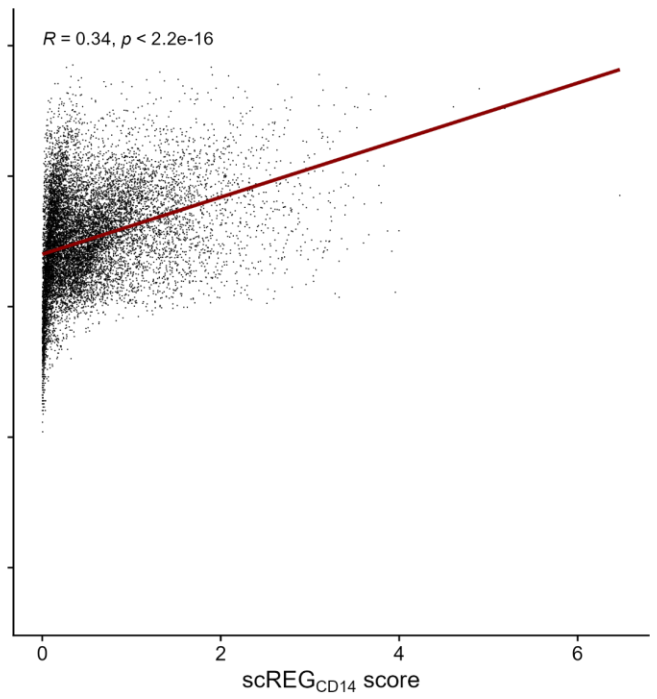
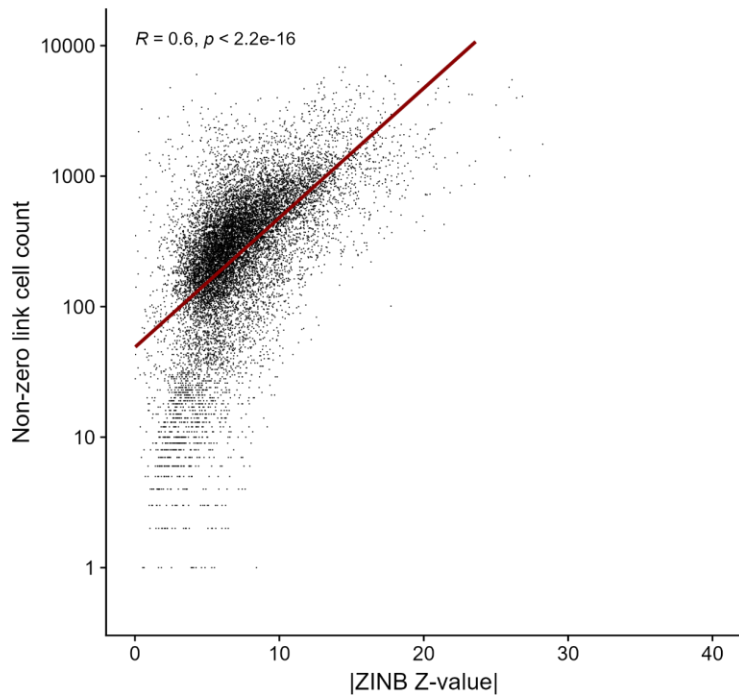
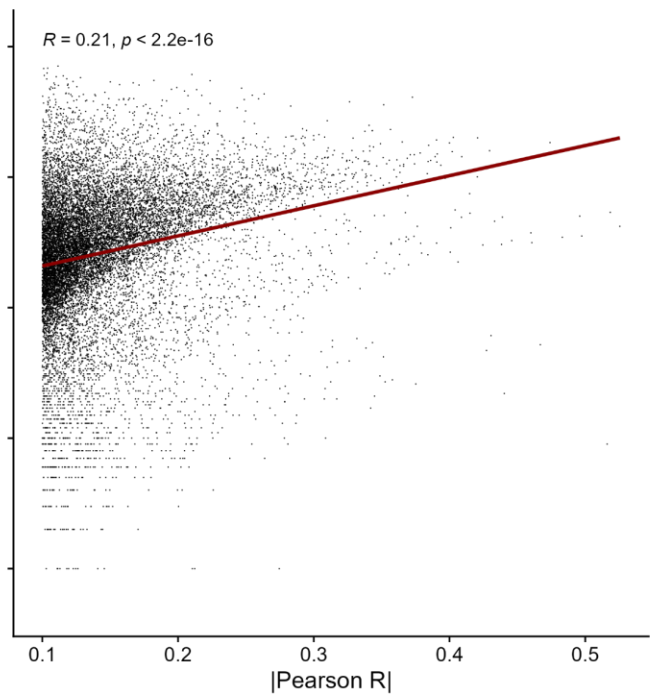
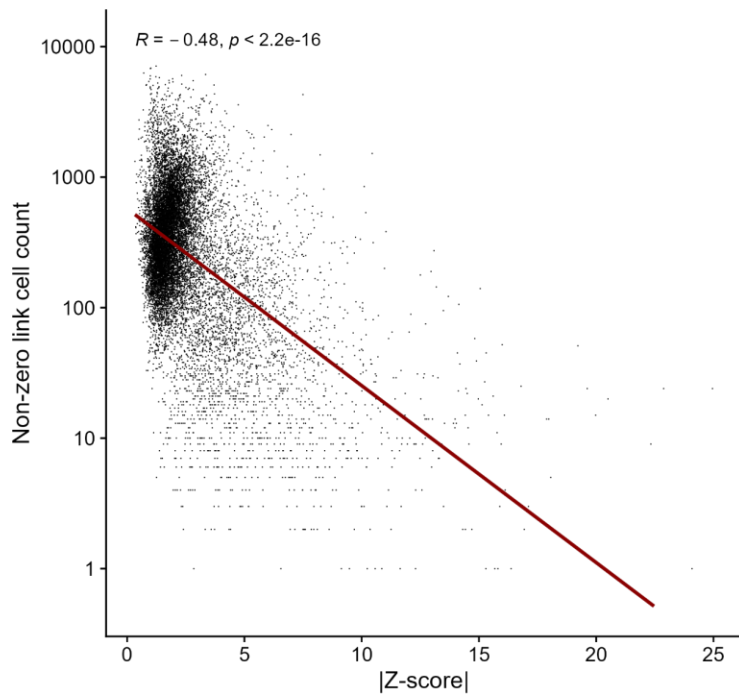


Supplementary Figure 3. The impact of cell-type counts on properties of the Z-scores method implemented in Signac. For cell-type-specific ATACseq peaks, we identified peak-gene links and compared (A) the most extreme P-value from the Z-score method, (B) the median P-value from the Z-score method, or (C) the percentage of bimodal null distributions with the number of cells in that cell-type. P-values are from the Spearman correlation test. Mono; Monocytes, cDC; classical Dendritic cells, NK; Natural killer cells, pDC; progenitor Dendritic cells, TEM; T effector memory cells, TCM; T central memory cells, gdT; Gamma delta ($\gamma\delta$) T cells, MAIT; mucosal-associated invariant T cells, Treg; regulatory T cells.

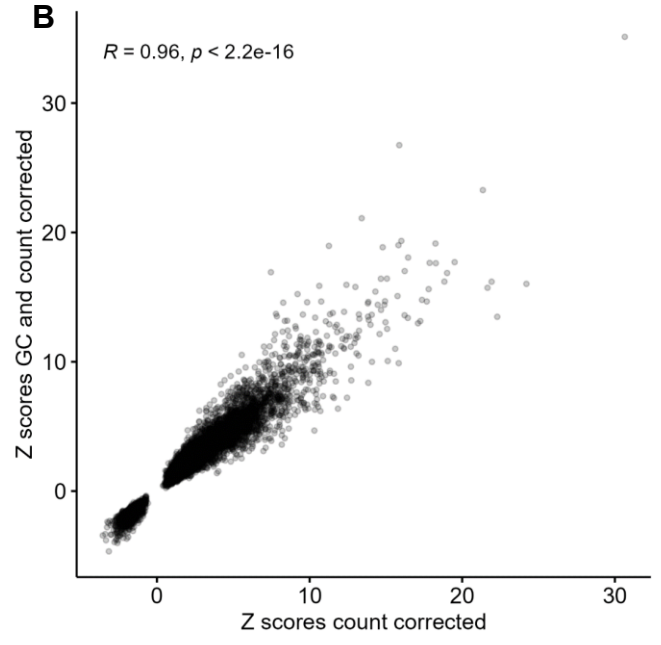
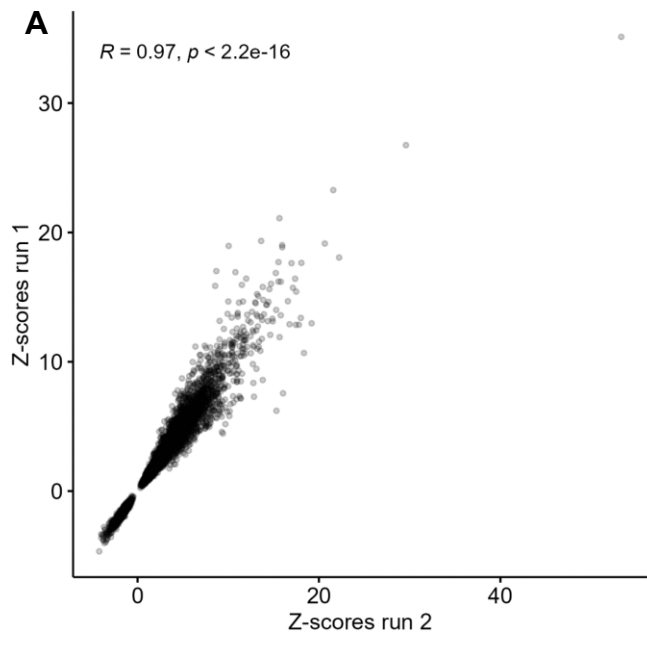
A**All peaks in background****B****No specific peaks in background**

Null distributions of 1000 matching peaks

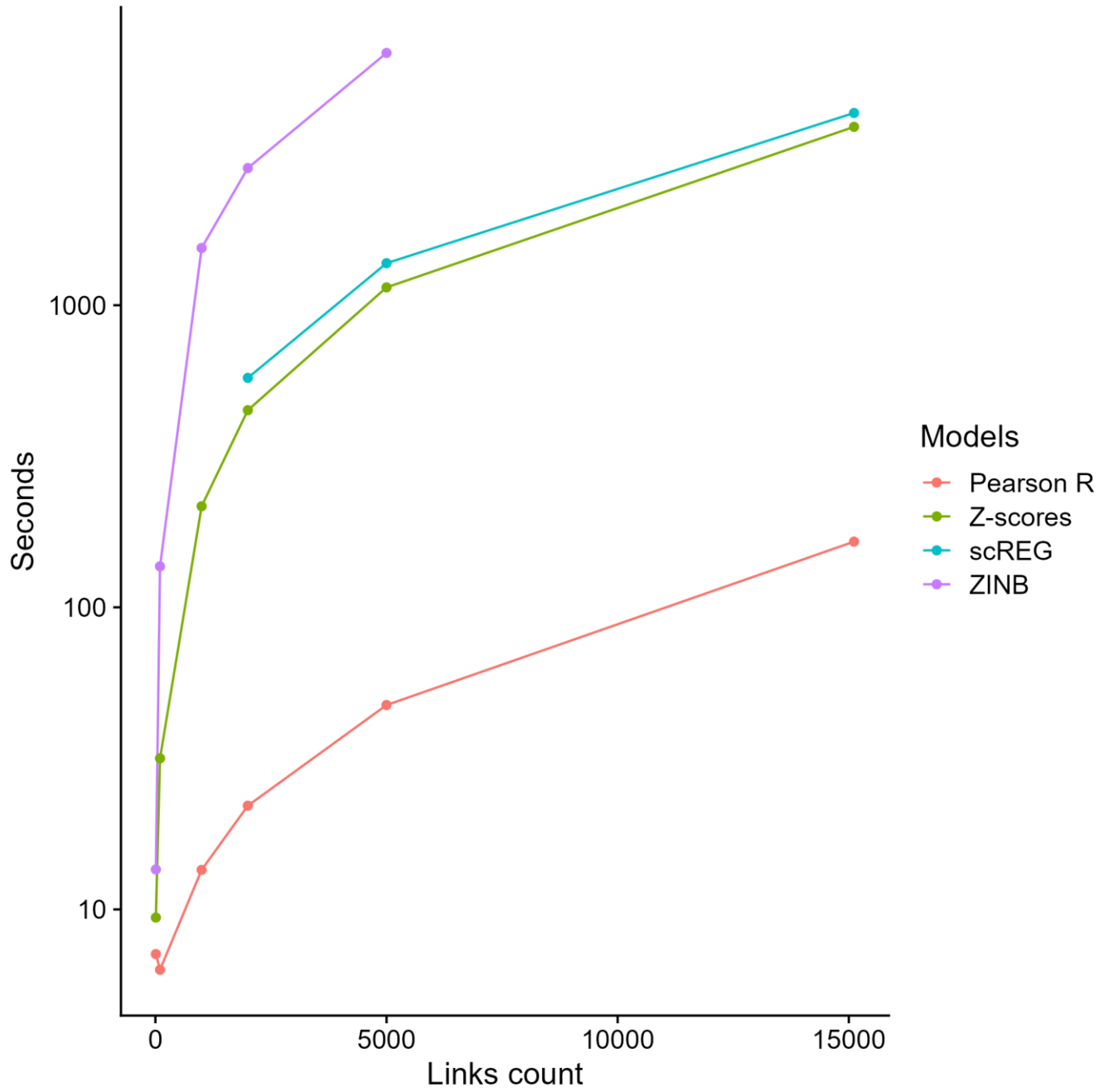
Supplementary Figure 4. Other examples of bimodal null distributions generated by the Z-scores method. Four GC- and count-matched null distributions with high Pearson R coefficients and low Z-scores. Labeled boxes represent the Z-scores for the tested cCRE and its linked gene (*y*-axis names: *gene_peak*) against the null distributions (**A**) before and (**B**) after removing from the dataset *trans* ATACseq peaks that are specific to the cell-type in which the cCRE is mostly accessible.



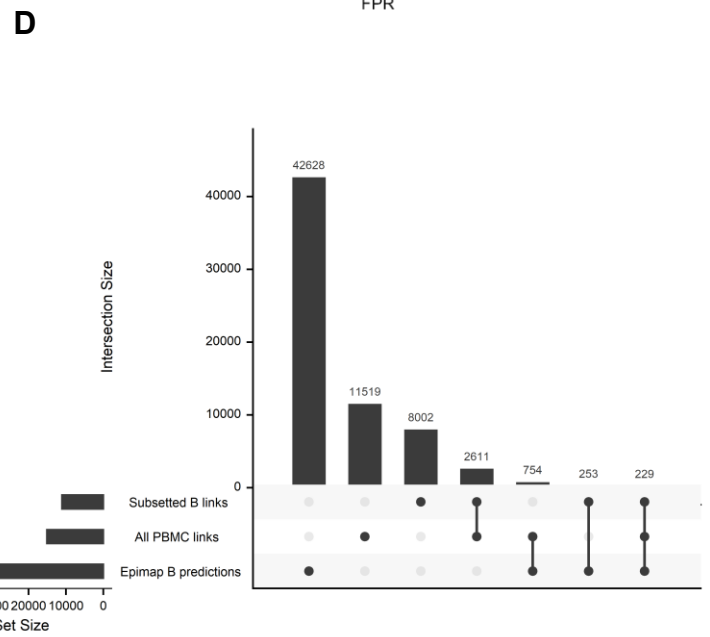
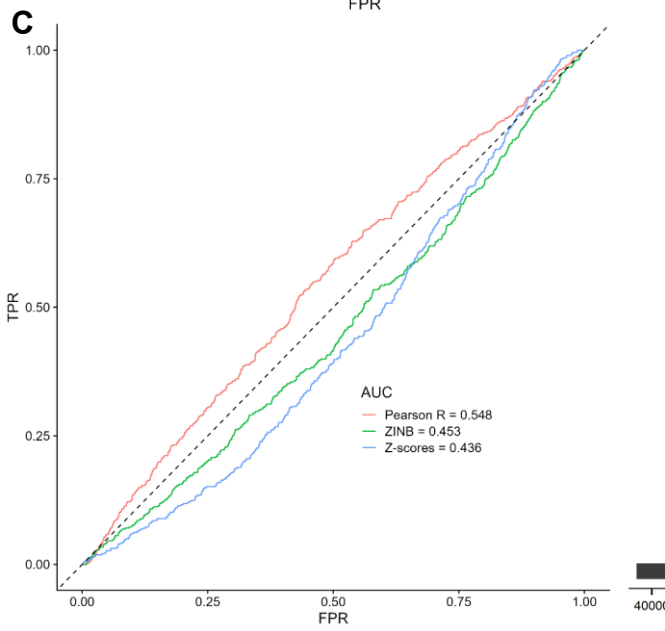
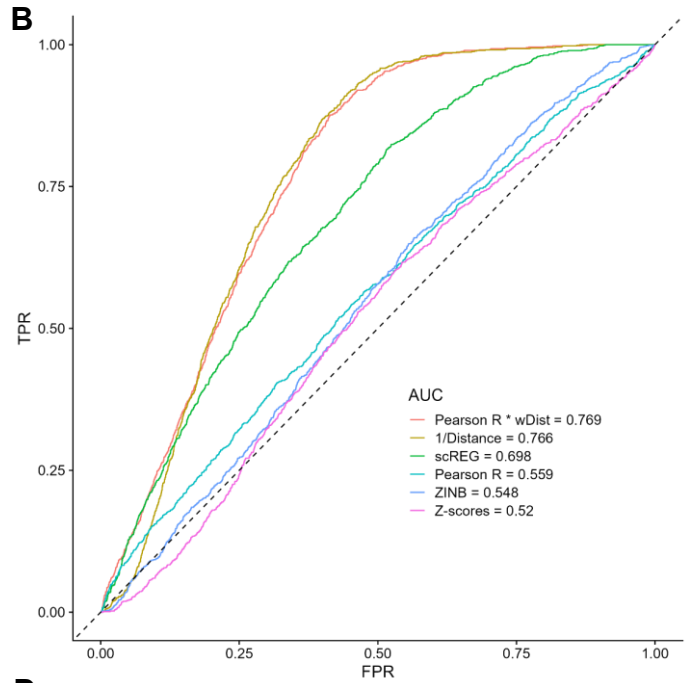
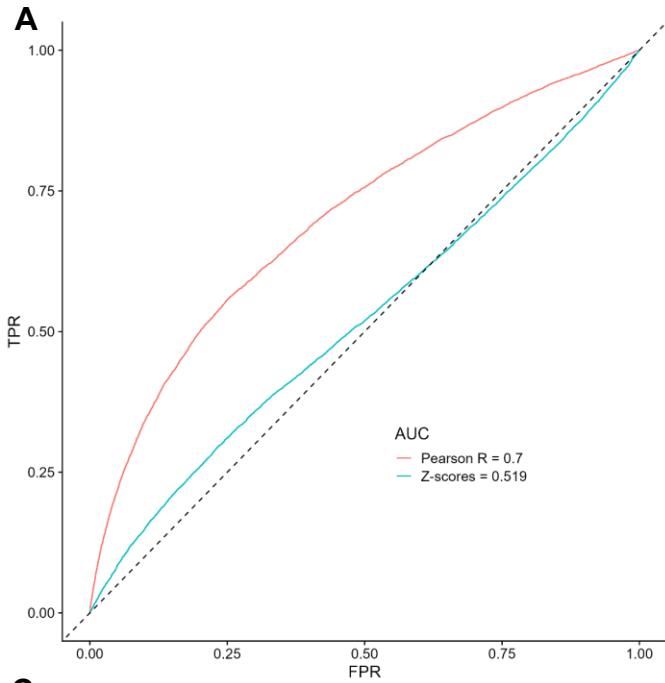
Supplementary Figure 5. The Z-scores method tends to output extreme statistics for peak-gene links that are identified in a few cells. In contrast, the statistics for the Pearson R, ZINB and scREG_{CD14} methods are higher when there are more cells with non-zero counts (as expected given higher power to detect links). Z-scores, ZINB Z-values and Pearson R from links with $|\text{Pearson R}| > 0.1$ were compared against the number of cells for which both the gene and the peak from that link had a non-zero read count. We found one outlier using ZINB which was removed for visualisation. On each plot, we added the Pearson R coefficient and corresponding P-value.



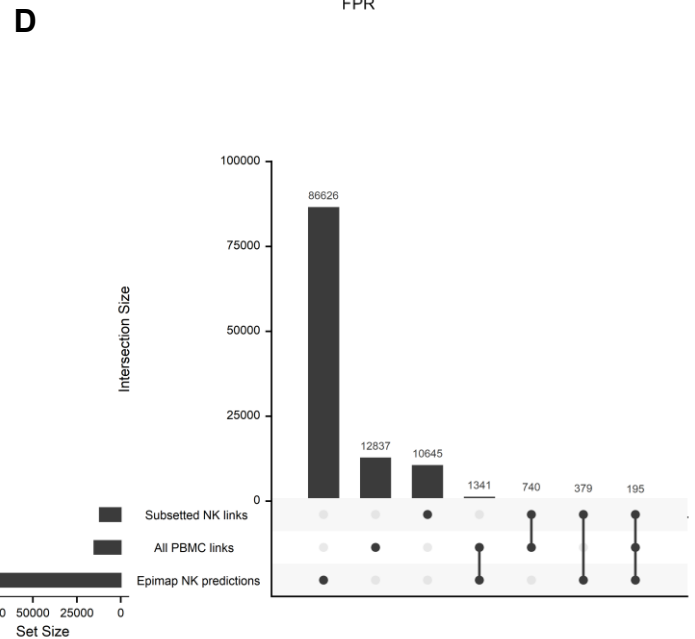
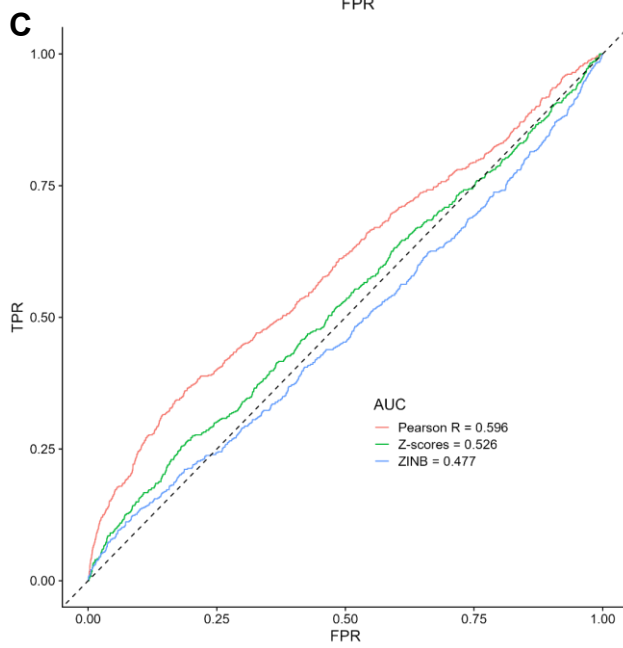
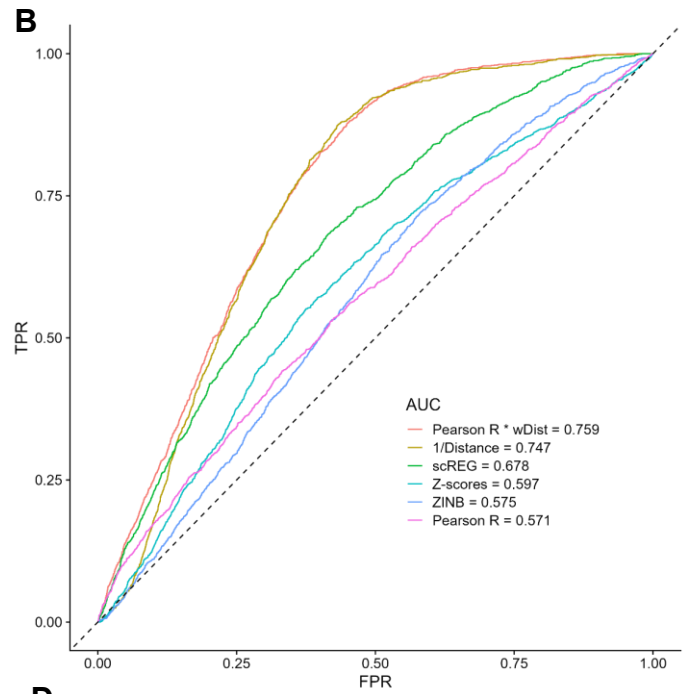
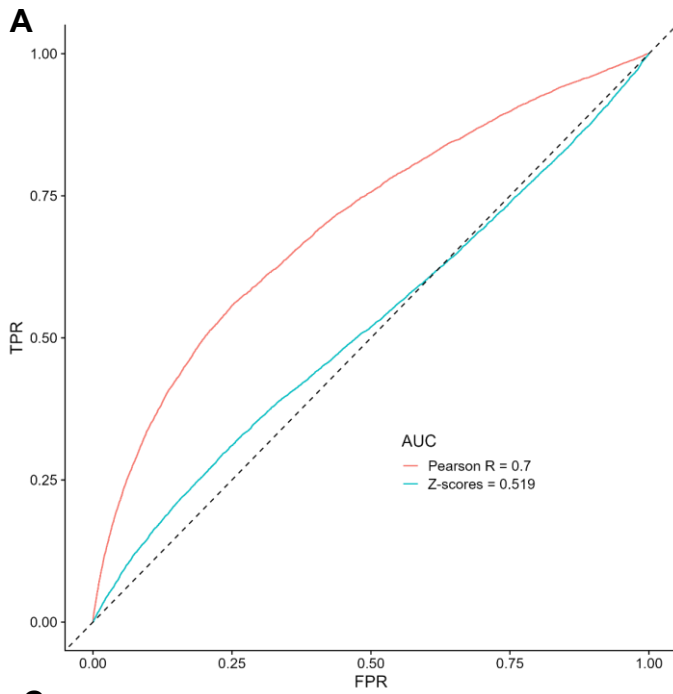
Supplementary Figure 6. Accounting for GC content has minimal impact on the peak-gene link statistics. **(A)** Distribution of Z-scores for 2 analyses of all peak-gene links with $|\text{Pearson R}| > 0.1$ using the same model. The variability is due to the stochastic sampling of peaks to create null distributions. **(B)** Distribution of statistics comparing the Z-scores model matching peaks for both GC percent and counts (y -axis) or counts only (x -axis). On each plot, we added the Pearson R coefficient and corresponding P-value.



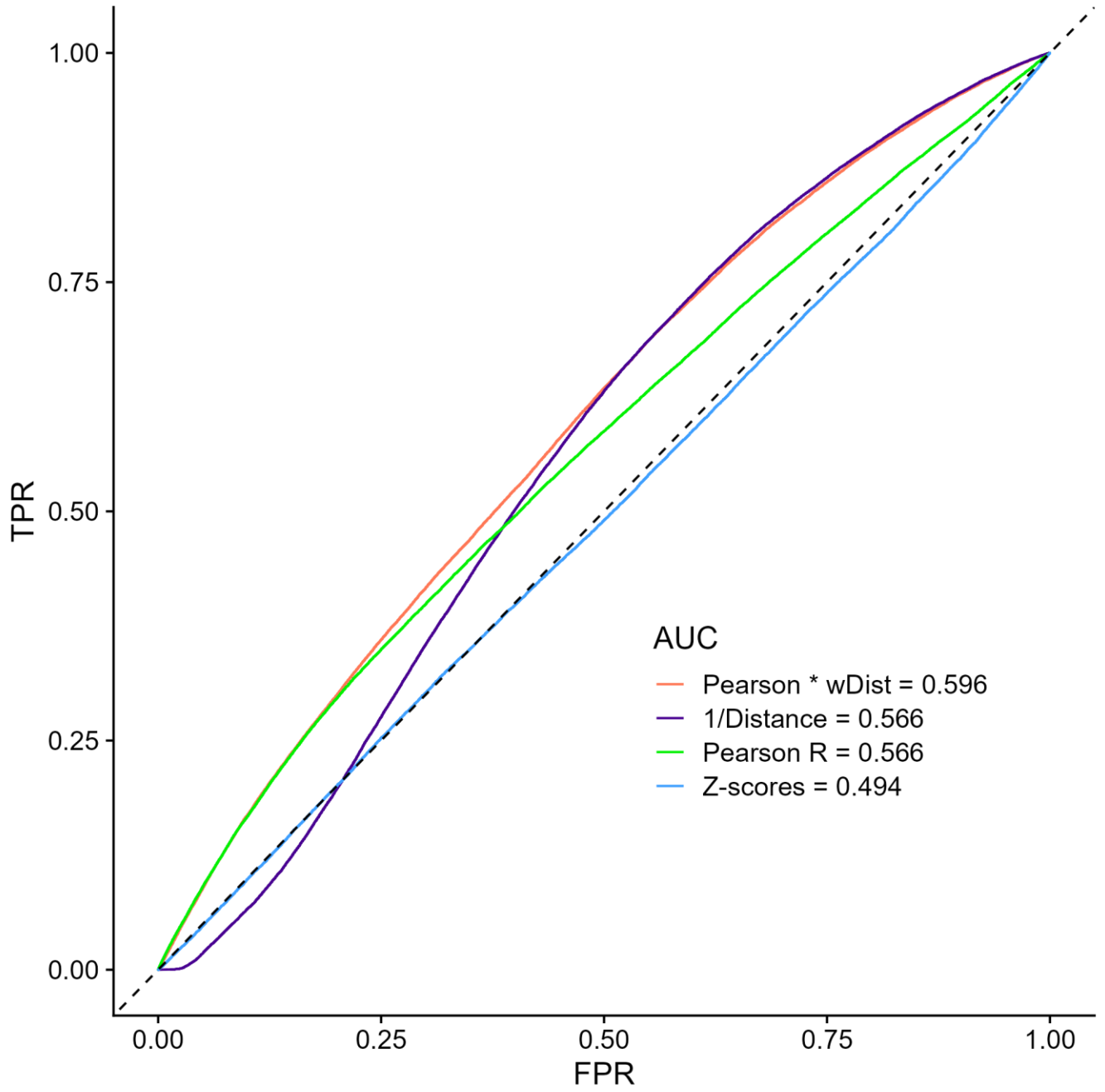
Supplementary Figure 7. The Pearson R provides an important scalability advantage. We benchmarked times to run each of the 4 models tested using 1 core with an AMD Ryzen 7 5800X 3,8GHz processor. For each model we tested 10, 100, 1000, 5000 and 15000 links except for ZINB which shows poor scalability. scREG returned errors for inputs with < 2000 links.



Supplementary Figure 8. The Pearson R method more accurately validates Epimap-predicted links between cCRE and target genes in B cells. **(A)** We used the Pearson R and Z-scores methods to detect links between ATACseq peaks and target genes (590,842 links with $|\text{Pearson R}| > 0.01$) in the complete (i.e., using all PBMC to compute statistics) PBMC multiomic dataset. Then, we performed Receiving Operating Curves (ROC) analyses to compare the identified peak-gene links from the multiomic data with regulatory links in B cells predicted by the Epimap Project. **(B)** As in **A**, but using a smaller set of links defined using a more stringent statistical threshold (15,113 links with $|\text{Pearson R}| > 0.1$). All cell-types are used to identify links, except for scREG which by design output link scores by cell-type (in this case, B cells). **(C)** As in **B**, but limiting these ROC analyses to links between ATACseq peaks and target genes with $|\text{Pearson R}| > 0.1$ that were found in the B cells subset of the PBMC multiomic dataset. **(D)** Upset plot that shows the intersections of links identified between ATACseq peaks and target genes using either the full PBMC multiomic dataset or only the B cells subset with cCRE-gene regulatory links in B cells as predicted by the Epimap Project. ZINB; zero-inflated negative binomial, wDist; weighted distance ($e^{-\text{distance}/200\text{kb}}$), TPR, true positive rate; FPR, false positive rate.



Supplementary Figure 9. The Pearson R method more accurately validates Epimap-predicted links between cCRE and target genes in NK cells. **(A)** We used the Pearson R and Z-scores methods to detect links between ATACseq peaks and target genes (590,842 links with $|\text{Pearson R}| > 0.01$) in the complete (i.e., using all PBMC to compute statistics) PBMC multiomic dataset. Then, we performed Receiving Operating Curves (ROC) analyses to compare the identified peak-gene links from the multiomic data with regulatory links in NK cells predicted by the Epimap Project. **(B)** As in **A**, but using a smaller set of links defined using a more stringent statistical threshold (15,113 links with $|\text{Pearson R}| > 0.1$). All cell-types are used to identify links, except for scREG which by design output link scores by cell-type (in this case, NK cells). **(C)** As in **B**, but limiting these ROC analyses to links between ATACseq peaks and target genes with $|\text{Pearson R}| > 0.1$ that were found in the NK cells subset of the PBMC multiomic dataset. **(D)** Upset plot that shows the intersections of links identified between ATACseq peaks and target genes using either the full PBMC multiomic dataset or only the NK cells subset with cCRE-gene regulatory links in NK cells as predicted by the Epimap Project. ZINB; zero-inflated negative binomial, wDist; weighted distance ($e^{-\text{distance}/200\text{kb}}$), TPR, true positive rate; FPR, false positive rate.



Supplementary Figure 10. The Pearson R method more accurately validates PChi-C-predicted links. We used the Pearson R and Z-scores methods to detect links between ATACseq peaks and target genes (590,842 links with $|\text{Pearson R}| > 0.01$) in the PBMC multiomic dataset. Then, we performed Receiving Operating Curves (ROC) analyses to compare the identified peak-gene links from the multiomic data with links found in PChi-C (see Methods). wDist; weighted distance ($e^{-\text{distance}/200\text{kb}}$), TPR, true positive rate; FPR, false positive rate.